Novel and conventional inhibitors of canonical autophagy differently affect LC3-associated phagocytosis

Stempels, Femmy C; Janssens, Maaike H; Ter Beest, Martin; Mesman, Rob J; Revelo, Natalia H; Ioannidis, Melina; van den Bogaart, Geert

Published in:
FEBS Letters

DOI:
10.1002/1873-3468.14280

Publication date:
2022

DR. GEERT VAN DEN BOGAART (Orcid ID : 0000-0003-2180-6735)

Received Date : 07-Sep-2021
Revised Date : 06-Dec-2021
Accepted Date : 23-Dec-2021
Article type : Research Article

Novel and conventional inhibitors of canonical autophagy differently affect LC3-associated phagocytosis

Femmy C. Stempels[1], Maaike H. Janssens[1], Martin ter Beest[2], Rob J. Mesman[3], Natalia H. Revelo[2], Melina Ioannidis[1], Geert van den Bogaart[1,2,*].

1 Department of Molecular Immunology, Groningen Biomolecular Sciences and Biotechnology Institute, University of Groningen, Groningen, The Netherlands.
2 Department of Tumor Immunology, Radboud Institute for Molecular Life Sciences, Radboud University Medical Center, Nijmegen, The Netherlands
3 Department of Microbiology, RIBES, Faculty of Science, Radboud University Nijmegen, Nijmegen, The Netherlands

*** Correspondence:**
Geert van den Bogaart
ORCID: 0000-0003-2180-6735

University of Groningen
Department of Molecular Immunology
Nijenborgh 7, 9747 AG Groningen
Email: G.van.den.Bogaart@rug.nl
Tel: +31 50 363 2150
Fax: +31 50 363 2154

Keywords:
LC3-associated phagocytosis, LAP, autophagy, chloroquine, bafilomycin A1, EACC, SAR405

Abstract

In autophagy, LC3-positive autophagophores fuse and encapsulate the autophagic cargo in a double-membrane structure. In contrast, lipidated LC3 (LC3-II) is directly formed at the phagosomal membrane in LC3-associated phagocytosis (LAP). In this study, we dissected the effects of autophagy inhibitors on LAP. SAR405, an inhibitor of VPS34, reduced levels of LC3-II and inhibited LAP. In contrast, the inhibitors of endosomal acidification bafilomycin A1 and chloroquine increased levels of LC3-II, due to reduced degradation in acidic lysosomes. However, while bafilomycin A1 inhibited LAP, chloroquine did not. Finally, EACC, which inhibits the fusion of autophagosomes with lysosomes, promoted LC3 degradation possibly by the proteasome. Targeting LAP with small molecule inhibitors is important given its emerging role in infectious and autoimmune diseases.

List of acronyms

CHX: cycloheximide;
DC: dendritic cell;
EBSS: Earle's balanced salt solution;
EGF: epidermal growth factor;
FBS: fetal bovine serum;
HOPS: homotypic fusion and protein sorting;
LAP: LC3-associated phagocytosis;
PBMC: peripheral blood monocyte;
PI(3)P: phosphatidylinositol 3-phosphate;
PI3K: phosphoinositide 3-kinase;
ROS: reactive oxygen species;
SLE: systemic lupus erythematosus.

Introduction

LC3-associated phagocytosis (LAP) plays critical roles in the immune system (Fazeli and Wehman, 2017; Herb et al., 2020; Wong et al., 2018; Wu and Lu, 2019). LAP is a non-canonical mechanism of autophagy, where the non-lipidated form of the ATG8 protein family member LC3 (MAP1LC3B), called LC3-I, becomes tethered at the single enclosing membrane of phagosomes by its direct conjugation to the lipids phosphatidylethanolamine and possibly also phosphatidylserine (Durgan et al., 2021), forming the lipidated form called LC3-II (Sanjuan et al., 2007). LAP is a common phenomenon in macrophages and dendritic cells (DCs), as LC3-positive phagosomes, called LAPosomes, have been observed for multiple phagocytic cargoes and for intracellular pathogens residing within membrane-encapsulated vacuoles (Lamprinaki et al., 2017; Martinez et al., 2011, 2015; Sanjuan et al., 2007). LAP helps to clear pathogens via engulfment and phagosome acidification (Herb et al., 2020; Martinez et al., 2015; Sanjuan et al., 2007), offers protection against intracellular pathogens such as *Listeria monocytogenes* (Gluschko et al., 2018) and *Salmonella* (Masud et al., 2019a), and enhances MHC class II presentation (Ligeon et al., 2021; Romao et al., 2013). Moreover, LAP promotes type 1 interferon production upon engagement of Toll-like receptor 9 molecules present in LAPosomes, by facilitating the recruitment of kinase IKK and adapter protein TRAF3 and transcription factor IRF7 (Hayashi et al., 2018). LAP also plays a role in the clearance of cell corpses and other cellular debris (Martinez et al.,

2011), and mice with dysfunctional LAP develop systemic lupus erythematosus (SLE)-like symptoms after injection with apoptotic cells (Martinez et al., 2016). In contrast to these beneficial effects, LAP can induce tumour immune tolerance by promoting the production of anti-inflammatory cytokines after engulfment of dead cells (Cunha et al., 2018).

The cellular mechanisms that regulate LAP are increasingly well understood. The ubiquitin-like conjugation systems that anchor LC3 to the target membrane are the same for canonical autophagy and LAP (Herb et al., 2020; Martinez et al., 2015; Sanjuan et al., 2007). However, the activation mechanisms of these conjugation systems differ. In contrast to canonical autophagy, LAP does not rely on the ULK1/2 pre-initiation complex (Martinez et al., 2015). Instead, LAP is triggered by surface receptors, including pattern recognition receptors such as TLRs, C-type lectins, IgG receptors, and scavenger receptors (Gluschko et al., 2018; Herb et al., 2020; Romao et al., 2013; Sanjuan et al., 2007). Similar to the activation of the ULK1/2 complex in canonical autophagy, engagement of these surface receptors induces the production of the lipid phosphatidylinositol 3-phosphate (PI(3)P) in the target phagosomal membrane by a class III phosphoinositide 3-kinase (PI3K) complex (PI3KC3) (Backer, 2016). Many proteins associated with this PI3KC3 complex are shared between canonical autophagy and LAP, such as the PI(3)P-kinase VPS34, but there are some differences such as the association of the protein Rubicon with the PI3KC3 complex in LAP but not in canonical autophagy (Martinez et al., 2015; Masud et al., 2019b).

Another difference with canonical autophagy is the reliance of LAP on reactive oxygen species (ROS), particularly ROS produced by the phagosomal NADPH oxidase NOX2 (Gluschko et al., 2018; Huang et al., 2009; Martinez et al., 2015; Masud et al., 2019a; Romao et al., 2013). NOX2 is a large complex composed of the integral membrane components gp91^{phox} and p22^{phox} and cytosolic subunits p67^{phox}, p47^{phox}, p40^{phox} and Rac1/2. NOX2 activation is promoted by Rubicon, because the PI(3)P produced by Rubicon-containing PI3PKC3 promotes assembly of the NOX2 complex and because Rubicon binds and stabilizes p22^{phox} (Martinez et al., 2015; Yang et al., 2012). NOX2 then produces superoxide anion inside the lumen of LAPosomes, and this can last for hours after cargo uptake. Superoxide anion, and/or other forms of ROS derived from this, promote LAP by direct oxidative inactivation of the protease ATG4B (Ligeon et al., 2021). This inactivation prevents the ATG4B-mediated deconjugation of LC3-II from the phagosomal membrane (Ligeon et al., 2021).

The association of LC3-II with the LAPosome promotes the fusion with lysosomes, and thereby facilitates the degradation of the phagocytic cargo (Martinez et al., 2015). While the fusion of canonical autophagosomes with lysosomes is well understood (Vats and Manjithaya, 2019), less is known about the fusion of LAPosomes with lysosomes. Fusion of autophagosomes with lysosomes is mediated by the SNARE protein syntaxin-17 (Stx17), which, upon completion of formation of the autophagosome, inserts its C-terminal hairpin loop in the autophagosomal membrane (Itakura et al., 2012). Subsequently, Stx17 can interact with its cognate partner SNAREs SNAP29 and VAMP8 in the lysosomal membrane, resulting in the formation of a coiled-coil alpha-helical bundle that overcomes the energy barrier of membrane fusion of both organelles (Guo et al., 2014; Itakura et al., 2012). Stx17 has also been

identified in phagosomes in several proteomics studies (Dingjan et al., 2018), suggesting that it might also play a role in LAPosome-lysosome fusion.

The aim of this study was to determine the effects of two new inhibitors of autophagy on LAP in human DCs loaded with zymosan particles: the VPS34 inhibitor SAR405 (Ronan et al., 2014) and the Stx17 inhibitor ethyl (2-(5-nitrothiophene-2-carboxamido) thiophene-3-carbonyl) carbamate (EACC) (Vats and Manjithaya, 2019). We compared these inhibitors with two canonical inhibitors of autophagy: the V-ATPase inhibitor bafilomycin A1 and the lysosomotropic base chloroquine (Klionsky et al., 2021; Pasquier, 2016). First, we confirmed that LC3 is recruited to the single membrane of DC phagosomes by using electron microscopy on cells that were cryofixed with high-pressure freezing. We found that whereas bafilomycin A1 increased and SAR405 reduced the cellular levels of LC3-II, both compounds resulted in a reduced recruitment of LC3 to phagosomes. In contrast, chloroquine, which increases the content of LC3-II in a similar fashion to bafilomycin A1, did not affect the phagosomal recruitment of LC3. Finally, treatment with EACC lowered the total cellular levels of both LC3-I and LC3-II, and co-incubation experiments with bafilomycin A1 showed that this was irrespective of lysosomal acidification. Instead, co-incubation experiments with the proteasome inhibitor MG132 suggested that EACC increased LC3 degradation by the proteasome. Thus, all of these small molecule inhibitors differently affect the LC3 flux and LAP, and can hence be used to address different aspects of these phagocytic processes.

Methods

Generation of monocyte-derived DCs

Human monocyte-derived DCs were derived from peripheral blood monocytes (PBMCs) obtained from healthy individuals as described previously (Baranov et al., 2019). Approval to conduct experiments with human blood samples was obtained from the blood bank and all experiments were conducted according to national and institutional guidelines. Informed consent was obtained from all blood donors by the Dutch blood bank. Samples were anonymized and none of the investigators could ascertain the identity of the blood donors. Briefly, adherent monocytes isolated from the blood of healthy donors were differentiated into monocyte-derived DCs by culturing in RPMI 1640 medium supplemented with L-glutamine (Gibco, 21875-034), 10% fetal bovine serum (FBS) (Thermo Fisher, 10309433), 1% antibiotic-antimitotic (Gibco, 15240062), 300 U/mL interleukin-4 (Miltenyi, 130-093-924) and 450 U/mL granulocyte-macrophage colony-stimulating factor (Miltenyi, 130-093-867) for 6 days at 37°C and 5% CO_2. Cells were detached by incubating them in PBS at 4°C for 1 hour. Cells were resuspended in RPMI with 10% FBS and diluted 1:1 in freezing medium resulting in a final concentration of 10% DMSO and 40% FBS. Cells were frozen in liquid nitrogen for later use.

Western Blot

For the Western Blot experiments, 500,000 cells per well were plated in RPMI with 10% FBS in a 12 wells plate. Cells were incubated at 37°C and 5% CO_2 for 2 hours to recover from thawing. Then, the medium was replaced with RPMI without FBS unless stated otherwise. To investigate the effects of starvation, cells were incubated in RPMI containing FBS or FBS free Earle's balanced salt solution (EBSS) (Sigma, E7510) supplemented with 2.2 g/L sodium

bicarbonate. Zymosan A (Sigma, Z4250-1G) was added to the media at a concentration of 5 particles per cell. Small molecule inhibitors used were 250 nM bafilomycin A1 (Invivogen, tlrl-baf1), SAR405 (Axon Medchem, 2716, concentrations as indicated), 25 μM chloroquine (Sigma, C-6628) or EACC (Life Chemicals Europe GmbH, F1385-0554, concentrations as indicated). To the control samples, DMSO was added in a concentration equal to the highest DMSO concentration in the experimental samples (solvent control). Cells were incubated at 37°C and 5% CO_2 for 4 hours or as indicated. For the experiments with MG132 (25 μM, Sigma, M7449), and/or cycloheximide (150 μM, Sigma, C7698), cells were pre-incubated for 1 hour with these inhibitors prior to adding zymosan A and/or EACC. In addition, MG132 and cycloheximide were present during the 4 hour incubation. Subsequently, cells were lysed in 20 mM Tris-HCl pH 7.6, 137 mM NaCl, 1% IGEPAL, 2 mM EDTA with phosphatase inhibitors (Roche, 4906837001) and protease inhibitors (Roche, 11697498001). Lysates were run on 12% SDS –polyacrylamide gels. Blots were probed with polyclonal rabbit anti-LC3B IgG (Novus Biologicals, NB600-1384), monoclonal mouse anti-mono- and -polyubiquitinylated conjugates IgG1 (clone UBCJ2, Enzo Life Sciences, ENZ-ABS840), monoclonal rabbit anti-GAPDH IgG (clone 14C10, Cell signaling, 2118) or monoclonal rat anti-tubulin IgG2a (clone YOL1/34, Novus Biologicals, NB100-1639), all at 1:1000. Subsequently, blots were labeled with goat anti-rat IgG (H+L) Alexa Fluor 680 (Thermo Fisher, A-21096), goat anti-rat IgG IRDye800CW (LI-COR, 925-32219), goat anti-mouse IgG IRDye800CW (LI-COR, 926-32210), donkey anti-rabbit IgG IRDye680CW (LI-COR, 926-32223) or goat anti-rabbit IgG IRDye800CW (LI-COR, 926-32211), all at 1:10,000. Blots were scanned using the Odyssey CLx Infrared Imaging System, and analysed in ImageStudio (both Li-Cor).

Immuno-electron Microscopy

Cells were thawed and resuspended in RPMI supplemented with 10% FBS and 1% antibiotic-antimitotic. Cells were then plated on circular Aclar discs (4 mm diameter) previously coated with 10 μg/ml fibronectin and pasted to the bottom of a 12-well plate well. Each well contained three discs and received 300,000 cells in 1 ml of medium. After 30 minutes of attachment at 37°C and 5% CO_2, the medium was replaced with RPMI medium without FBS for an additional 30 minutes. Subsequently, the medium was replaced with new RPMI medium without FBS, containing 5 zymosan particles/cell, and cells were incubated for another 30 minutes. Medium was removed and replaced with Leibovitz's L-15 medium (Gibco, 21083-027) supplemented with L-glutamine but lacking serum to maintain the cells during the preparation of the high-pressure freezing procedure. Before freezing, each coverslip was dipped in a solution of 0.5% ultra-low gelling temperature agarose dissolved in Leibovitz's L-15 medium to ensure that the cells would not detach, then placed in a 6 mm platelet carrier and immediately high-pressure frozen in a Leica EM HPM-100 (Leica Microsystems). Samples were then transferred to a flow-through sample embedding mold under liquid nitrogen and freeze-substituted using an AFS2 device (Leica Microsystems). Substitution was done with anhydrous acetone containing 0.1% uranyl acetate. The substitution protocol started at −90°C for 48 h, then rising to −70°C within 20 h, maintaining the temperature at −70°C for 12 h, then rising to −50°C within 20 h and staying at −50°C for 12 h. Samples were then washed twice for 30 minutes with anhydrous acetone at −50°C. Resin infiltration was performed in steps of increasing concentrations of 25%, 50%, 75% and 100% Lowicryl HM20 (Electron Microscopy Sciences, Hatfield PA, USA) dissolved in anhydrous acetone accordingly, each step of one hour at −50°C. This was followed by a 12-hour incubation in 100% Lowicryl HM20 and three washes of one hour each with 100% Lowicryl

HM20, all at −50°C. Finally, samples were polymerized in fresh 100% Lowicryl HM20 under UV light for 144 hours. Samples were then sectioned with a Leica Ultracut UCT ultramicrotome (Leica Microsystems) in 70 nm thick sections and placed on 100 mesh formvar- and carbon-coated copper grids (Electron Microscopy Sciences). For immunogold labeling, grids were first rinsed 5 times on drops of 0.1 M PHEM buffer (60 mM PIPES, 25 mM HEPES, 10 mM EGTA, 2 mM $MgCl_2$ at pH 6.9) for 2 minutes each, and then blocked for 15 minutes in 0.1 M PHEM + 1% BSA. Subsequently, grids were labeled for 2 hours with rabbit anti-LC3B IgG (Cell Signaling, 2775S) diluted at 1:200 in 0.1 M PHEM + 1% BSA in a humidified chamber. Grids were washed five times for 2 minutes with 0.1 M PHEM + 0.1% BSA and then labeled for 2 hours with a solution of Protein A conjugated to 10 nm gold particles diluted at 1:200 in 0.1 M PHEM + 1% BSA (kindly provided by Jack A. Fransen, Radboud UMC, Nijmegen, The Netherlands). Thereafter, grids were washed five times with 0.1 M PHEM + 0.1% BSA and five times with 0.1M PHEM, fixed for 5 minutes with 1% glutaraldehyde in 0.1 M PHEM buffer and rinsed 10 times with distilled water. Finally, grids were poststained with 2% Uranyl acetate and Reynolds lead citrate. Grids were analysed with a JEOL JEM-1400 Flash transmission electron microscope (JEOL, Tokio, Japan).

Labeled zymosan A

Zymosan A (Sigma, Z4250-1G) was labeled with Alexa Fluor 405 by resuspending 85 mg zymosan in 900 µl Na_2CO_3 / $NaHCO_3$ 0.2 M pH 9.2 and subsequently incubating on a rotator with 100 nmol Alexa Fluor 405 succinimidyl ester (Thermo Fisher, Molecular Probes 10153622) for 90 minutes at room temperature while kept in the dark. To remove unbound fluorophores, zymosan was washed with PBS for 6 times.

Zymosan A (Sigma, Z4250-1G) was labeled with Bodipy 581/591 C11 (Invitrogen, 10257152) by resuspending 85 mg zymosan in 1 mL of Bodipy that was previously diluted in PBS at 1:100. Subsequently, the mixture was incubated for 1 hour on a rotator at room temperature while kept in the dark and washed 6 times with PBS to remove unbound Bodipy.

Assessment of LC3-recruitment to phagosomes

For the microscopy experiments, 50,000 cells were plated on 12 mm-diameter glass coverslips in RPMI medium with 10% FBS. Cells were incubated at 37°C and 5% CO_2 for 2 hours to recover from thawing. Afterwards, a preincubation with 100 nM bafilomycin A1, 10 µM SAR405, 25 µM chloroquine or 5 µM EACC was performed in cold RPMI for 30 minutes at 4°C. To the control samples, DMSO was added equal to the highest DMSO concentration in the experimental samples. Subsequently, the cells were incubated for 45 minutes at 37°C, 5% CO_2 in fresh RPMI containing the inhibitors and Alexa Fluor 405-labeled zymosan A particles (5 particles per cell). The plate was agitated every 10 minutes to prevent dissipation of the oxygen in the medium for optimal ROS production. Cells were fixed in 4% paraformaldehyde (PFA) for 15 minutes at room temperature and blocked and permeabilised in PBS with 20 mM glycine, 3% (w/v) BSA and 0,1% (w/v) saponin for 1 hour at room temperature. Cells were incubated with mouse monoclonal anti-NOX2 IgG1 (clone 7D5, MBL, D162-3) and polyclonal rabbit anti-LC3B IgG (Cell Signaling, 2775S), both at 1:200 dilution, for overnight at 4°C. Subsequently, cells were washed in PBS three times and coverslips were incubated for 1 hour at room temperature with the following secondary antibodies: donkey anti-mouse IgG (H+L) Alexa Fluor 647 (Thermo Fisher, Invitrogen, A31571) and donkey anti-rabbit IgG (H+L) Alexa

Fluor 488 (Thermo Fisher, Invitrogen, A21206), both at 1:800 dilution. For actin labeling, phalloidin Alexa Fluor 546 was used (Thermo Fisher, A22283) at 1:200 dilution. Cells were mounted in 70% glycerol with 4',6-diamidino-2-phenylindole (DAPI). Samples were imaged with a LSM800 Zeiss confocal laser scanning microscope with a 63x 1.4 NA oil immersion objective. Images were analyzed in Fiji (ImageJ) using the macro as described in Supplementary Fig. 3 and the supplementary information.

Viability, phagocytic efficiency and phagosomal oxidation measurements

In a 96-wells plate, 100,000 cells were seeded per well in 100 µl of RPMI supplemented with 10% FBS. Cells were incubated at 37°C and 5% CO_2 for 2 hours to recover from thawing. Afterwards, a preincubation with 100 nM bafilomycin A1, 10 µM SAR405, 25 µM chloroquine, 5 µM EACC or 100 µM α-tocopherol (Sigma, T3251) was performed in cold RPMI for 30 minutes at 4°C. To the control samples, DMSO was added in a concentration equal to the highest DMSO concentration in the experimental samples (solvent control). Subsequently, the cells were incubated for 1 hour at 37°C, 5% CO_2 in fresh RPMI containing the inhibitors and either Alexa Fluor 405-labeled zymosan A particles or Bodipy581/591 C11-labeled zymosan A particles (5 particles/cell). Cell viability was assessed with the fixable viability dye eFluor780 (ThermoFisher; 65-0865-18) at 1:200 in PBS for 10 minutes on ice prior to 4% PFA fixation. Cells were run at a CytoFlex S Flow Cytometer (Beckman Coulter). Analysis was performed in FlowJo. Phagosomal oxidation was determined from the ratio of the fluorescence signals of the oxidized Bodipy581/591 C11 dye (emission in the FITC channel) over those of the non-oxidized dye (emission in the PE channel). As the dye was coupled to the zymosan particles (i.e., the phagocytic cargo), changes in phagocytic efficiency will not affect this ratio.

RNA isolation, cDNA synthesis and qPCR

In a 6-well plate, 500,000 cells were seeded per well in RPMI with 10% FBS. Cells were incubated at 37°C and 5% CO_2 for 2 hours to recover from thawing. RPMI lacking FBS was used to wash the cells before treating them for 4 hours with FBS free RPMI containing DMSO, 5 µM EACC or 10 µM EACC. RNA isolation was performed using the Quick-RNA MiniPrep kit (ZymoResearch, R1054) in accordance with the manufacturer's instructions. For generating cDNA, the Moloney murine leukemia virus reverse transcriptase (M-MLV-RT) kit (Invitrogen, 28025-021) was used following the manufacturer's instructions. After cDNA synthesis, qPCR was performed using 5 µL Sybr Green Master Mix (Applied biosystems, A25742) and the following primers: Housekeeping gene *SNRPD3* forward 5'-GGAAG CTCAT TGAAG CAGAG GAC -3' and reverse 5'-CAGAA AGCGG ATTTT GCTGC CAC-'3; *MAP1LC3B* forward 5'-CCGCA CCTTC GAACA AAGAG-'3 and reverse 5'-TTGAG CTGTA AGCGC CTTCT-'3. The qPCR-program consisted of the following steps: 50°C for 2 minutes, 95°C for 2 minutes, 95°C for 15 seconds and 60°C for 1 minute. This program was repeated 40 times. The results were analyzed using the $2^{-\Delta\Delta Ct}$ method described by Livak and Schmittgen (Livak and Schmittgen, 2001).

Statistical Analysis

Data from individual donors are plotted in the graphs. The Western blot data was analyzed using a 1-way ANOVA followed by a post hoc Tukey test when required or a 2-way ANOVA followed by a post hoc Dunnett's test.

Microscopy data was analyzed using Student's paired two-sided t-tests. A p value < 0.05 was regarded as statistically significant (∗p < 0.05, ∗∗p < 0.01, ∗∗∗p < 0.001, ∗∗∗∗p < 0.0001).

Results

SAR405 inhibits LC3 lipidation, while EACC promotes LC3 degradation

We tested how LC3 lipidation and turnover were affected by four small molecule inhibitors that target different stages of autophagy: the inhibitor of the V-ATPase bafilomycin A1, the lysosomotropic base chloroquine, the VPS34 inhibitor SAR405 (Ronan et al., 2014), and the inhibitor of Stx17 EACC (Vats and Manjithaya, 2019). We addressed lipidation in DCs derived from monocytes isolated from human blood and tested the drugs at concentrations where the viability of the cells was not negatively affected (Supplementary Fig. 1). LC3-II generation and turnover can be measured by Western blot, because blocking of LC3-I lipidation results in lower levels of LC3-II, while blocking of lysosomal degradation results in elevated levels of LC3-II (Klionsky et al., 2021). Indeed, bafilomycin A1, which blocks the degradation of LC3-II in acidic lysosomes (Klionsky et al., 2021), resulted in increased levels of LC3-II (Fig. 1A; Supplementary Fig. 2A), as reported previously (Fischer et al., 2020; Florey et al., 2015; Guo et al., 2014; Jacquin et al., 2017). Moreover, zymosan particles, a phagocytic cargo that induces LAP (Sanjuan et al., 2007), also significantly increased LC3-II, albeit to lower levels than bafilomycin A1. In contrast, SAR405, which inhibits PI3KC3 upstream of LC3 lipidation, reversed the bafilomycin-mediated increase in LC3-II (Fig. 1A; Supplementary Fig. 2A), similar to reported previously in HeLa and H1299 cell lines (Ronan et al., 2014).

Chloroquine was originally believed to block autophagic flux through the same mechanism as bafilomycin A1, as it is a lysosomotropic base which inhibits the acidification of lysosomes and hence also inhibits the activity of lysosomal hydrolases (Jacquin et al., 2017; Poole and Ohkuma, 1981). However, more recently, it was shown that chloroquine mainly inhibits autophagy by impairing autophagosome fusion with lysosomes rather than by affecting the acidity and/or degradative activity of this organelle (Mauthe et al., 2018). We found that chloroquine increased the LC3-II accumulation, albeit to a somewhat lesser extent than bafilomycin A1 (Fig. 1B; Supplementary Fig. 2B), as reported previously (Gui et al., 2019; Mauthe et al., 2018).

The Stx17 inhibitor EACC is another compound that blocks autophagic flux by inhibiting the fusion of autophagosomes with lysosomes (Vats and Manjithaya, 2019). EACC treatment reduces the interaction of Stx17 with vacuolar protein sorting-associated protein 33A (VPS33A), a subunit of the regulatory homotypic fusion and protein sorting (HOPS) complex, and with its cognate SNARE complex partner vesicle-associated membrane protein 8 (VAMP8) in HeLa cells (Vats and Manjithaya, 2019). Since EACC also blocks the lysosomal degradation of LC3-II, it has been reported to increase the levels of LC3-II in starved HeLa cells (similarly to bafilomycin A1 and chloroquine) (Vats and Manjithaya, 2019). However, we did not observe such an accumulation of LC3-II in starved monocyte-derived DCs. In fact, when cultured in FBS free RPMI, both the levels of LC3-I and LC3-II decreased in a dose-dependent manner (Fig. 1C; Supplementary Fig. 2C, Supplementary Fig. 4). We also tested the effect of EACC in the presence of bafilomycin A1, because a further increase in the levels of LC3-II observed in the presence of both

these compounds, compared to bafilomycin A1 alone, would be indicative of an increased LC3 flux (Klionsky et al., 2021). However, also in the presence of bafilomycin A1, both LC3-I and LC3-II were reduced in a dose dependent manner upon treatment with EACC (Fig. 1D; Supplementary Fig. 2D). These findings show that EACC treatment reduces the cellular levels of LC3 irrespective of its lipidation and lysosomal acidification.

To investigate whether the EACC-induced decrease in LC3 levels is dependent on phagocytosis, we compared the effect of EACC in the presence and absence of zymosan, and used an EACC concentration of 5 μM, the lowest concentration where we observed a reduction in LC3 levels. Regardless of the presence of zymosan, we observed a significant reduction of LC3-I and a slight, non-significant reduction in LC3-II (Supplementary Fig. 3A-B). Since we found that blockage of lysosomal degradation with bafilomycin A1 did not affect the EACC-induced reduction in LC3 levels, we hypothesized that LC3 is degraded by the proteasome in the presence of EACC. To test this, we blocked the proteasome by (pre-)incubating the cells with 25 μM MG132. This concentration of MG132 does not affect the viability of monocyte-derived DCs (Verboogen et al., 2019). Both in the presence and absence of zymosan, the EACC-induced reduction in LC3-I levels did not further decrease when MG132 was also used, suggesting that proteasomal degradation might contribute to the decrease of LC3 (Supplementary Fig. 3A-B). We also tested whether EACC affects LC3 synthesis by blocking protein translation with 150 μM cycloheximide (CHX), a concentration that does not affect the viability of monocyte-derived DCs (Alvarez et al., 2009). Strikingly, cellular levels of both LC3-I and LC3-II were very low after 5 hours of incubation with CHX (1 hour of pre-incubation and 4 hours of incubation), pointing at a high turnover of LC3 in the cells. As the cells were not deprived of nutrients (they were incubated in RPMI which contains amino acids), this high turnover suggests that basal levels of autophagy are very high in monocyte-derived DCs. Although EACC did not further decrease the levels of LC3, these data are not conclusive given the low residual levels of LC3 in CHX treated cells. To further address this, we also investigated the effect of EACC on mRNA levels of the LC3 coding gene *MAP1LC3B* (Supplementary Fig. 3C). As neither 5 μM EACC nor 10 μM EACC affected the mRNA levels of *MAP1LC3B*, we conclude that EACC does not affect LC3 transcription. Thus, our data indicate that LC3 undergoes rapid turnover in monocyte-derived DCs and EACC promotes its degradation, possibly by the proteasome. This degradation is dependent on growth factors and nutrient availability, as EACC did not reduce LC3 levels in the presence of serum, and LC3 levels were already reduced in untreated cells (no EACC) maintained in minimal medium (EBSS) (Supplementary Fig. 4).

SAR405 and bafilomycin A1 inhibit LAP, whereas chloroquine and EACC do not affect LAP

In the next set of experiments, we addressed whether the autophagy inhibitors SAR405, EACC, bafilomycin A1 and chloroquine would affect LAP, thus the recruitment of LC3 to zymosan-containing phagosomes. We first observed recruitment of endogenous LC3 to the membrane of phagosomes using immunofluorescence confocal microscopy (Fig. 2A). Importantly, in contrast to the continuous signal around the phagosome given by GFP-tagged LC3, recruitment of endogenous LC3 always resulted in a punctuate staining juxtaposed to the phagosomes. Subsequently, we confirmed that indeed this signal was coming from the single-membrane of the phagosome using high-pressure freezing electron microscopy combined with immunogold labeling (Fig. 2B; Supplementary Fig. 5). We then tested the effect of these inhibitors on the phagocytosis efficiency of zymosan particles. Phagocytosis was significantly

inhibited by bafilomycin A1, SAR405 and chloroquine (Fig. 3). This might well be explained by a reduced endolysosomal trafficking, which is required for phagocytic uptake (Fairn and Grinstein, 2012), since the inhibition of endocytosis and/or pinocytosis has been observed for bafilomycin A1 (Xu et al., 2003), SAR405 (Filippakis et al., 2018) and chloroquine (Chen et al., 2011; Mauthe et al., 2018; Wolfram et al., 2017). For EACC, we did not observe any effect on the phagocytosis efficiency (Fig. 3), in line with previous findings that this compound does not affect endocytosis-mediated degradation of the epidermal growth factor (EGF) receptor (Vats and Manjithaya, 2019).

The recruitment of LC3 to phagosomes has been shown to depend on the activity of the NADPH oxidase NOX2 (Gluschko et al., 2018; Hooper et al., 2021; Huang et al., 2009; Ligeon et al., 2021; Martinez et al., 2015; Masud et al., 2019a; Romao et al., 2013). The integral membrane subunits of NOX2, consisting of gp91^{phox} and p22^{phox}, form a stable complex which is co-internalized with the plasma membrane during phagosome formation (Dingjan et al., 2017). We therefore reasoned that this membrane complex could be used as a marker for the phagosomal membrane during the stage of phagosomal maturation when LAP can be expected. We calculated the enrichment levels for both gp91^{phox} and LC3 by dividing the signal intensities of the immunofluorescence staining at the phagosomal membrane over the fluorescence signal in the cytoplasmic area immediately juxtaposed to the membrane (Supplementary Fig. 6 and Supplementary information). This analysis is insensitive to variations in protein levels and staining intensities between cells and donors. Immunofluorescence microscopy showed that about half of the phagosomes that contained LC3 also contained gp91^{phox} (Fig. 4A-B; compare grey and yellow curves). Gp91^{phox} and LC3 were both already present early after uptake (i.e., at the earliest assessed timepoint of 15 min), and gradually decreased over time (Fig. 4B). These findings indicate that indeed gp91^{phox} could be used as a marker for identification of phagosomes prone to LAP. In fact, the immunofluorescence signal levels of gp91^{phox} correlated with those of LC3 (Fig. 4C), strengthening the previous conclusion that the activity of NOX2 promotes LC3 recruitment (Ligeon et al., 2021; Masud et al., 2019a).

Next, we tested how the small molecule inhibitors chloroquine, bafilomycin, EACC and SAR405 would affect the recruitment of gp91^{phox} and LC3 to phagosomes (Fig. 5A). Bafilomycin A1 and SAR405 did not affect the recruitment of gp91^{phox} to the phagosomal membrane, as these compounds did neither affect the relative gp91^{phox} intensity at the membrane, nor the percentage of gp91^{phox}-positive phagosomes (relative intensity >1.1; Fig. 5B). Chloroquine resulted in a small, but significant, increase in the median relative gp91^{phox} intensity. In contrast, EACC significantly reduced the percentage of gp91^{phox}-enriched phagosomes, suggesting that Stx17 might play a role in gp91^{phox} trafficking. In line with these findings, we observed that EACC reduced phagosomal oxidation, while, compared to bafilomycin A1, chloroquine significantly increased oxidation (Fig. 6).

SAR405 reduced the phagosomal recruitment of LC3 (Fig. 5C). This is in line with expectations, because lipidation of LC3 is required for LAP (Herb et al., 2020; Martinez et al., 2015; Sanjuan et al., 2007). In addition, SAR405 has previously been shown to reduce the number of LAPosomes in human macrophages (Ligeon et al., 2021), although in this study the effect could also be attributed to the inhibition of uptake by SAR405. Even though bafilomycin A1 did not inhibit LC3-II formation (Fig. 1), it did inhibit LC3 recruitment to phagosomes (Fig. 5C). This is in line with

previous findings that LAP depends on the activity of the V-ATPase and can be inhibited by bafilomycin A1 (Florey et al., 2015; Hooper et al., 2021; Jacquin et al., 2017). Albeit not significant, EACC showed a tendency to also reduce phagosomal levels of LC3, as we observed a reduction in phagosomal content of LC3 in three out of four donors (Fig. 5C). This is possibly the result of the lower cellular levels of total LC3 caused by EACC (Fig. 1C). Finally, we did not observe a significant effect of chloroquine on the LC3 recruitment to phagosomes (Fig. 5C). This contradicts previous findings in murine macrophages, where it was reported that the osmotic destabilization of plain latex bead-containing phagosomes by chloroquine promoted the recruitment of LC3 to these phagosomes (Florey et al., 2015; Jacquin et al., 2017). We did not observe this for zymosan-containing phagosomes, but instead the phagosomal recruitment of LC3 even went down in three out of four donors (Fig. 5C).

Discussion

In this study, we addressed the effects of the small molecule inhibitors bafilomycin A1, chloroquine, SAR405 and EACC on cellular levels of LC3-I and its lipidated form LC3-II and on the occurrence of LAP in human monocyte-derived DCs (Fig. 7). We found that these inhibitors exert different effects on the flux of LC3: treatment with bafilomycin and chloroquine resulted in an increased presence of LC3-II, whereas SAR405 lowered the content of LC3-II, and EACC reduced the levels of both LC3-I and LC3-II. Bafilomycin A1 and SAR405 resulted in a decreased phagocytic efficiency, and LC3-II was recruited less to the phagosomes that were formed in the presence of either of these compounds, while phagosomal levels of $gp91^{phox}$ were not affected. Bafilomycin induced a (non-significant) trend towards decreased phagosomal oxidation. Chloroquine resulted in decreased phagocytosis efficiency, but did not affect the recruitment of LC3 to the phagosomes, while the recruitment of $gp91^{phox}$ and, compared to bafilomycin A1, phagosomal oxidation were somewhat increased. EACC did not affect the recruitment of LC3-II to phagosomes either, but in contrast to chloroquine, EACC decreased the percentage of $gp91^{phox}$-enriched phagosomes and reduced phagosomal oxidation, whereas it did not affect phagocytosis efficiency.

It has been reported that truncation mutants of LC3, which cannot be lipidated because they lack the required C-terminal residues, can be recruited to vacuoles containing the intracellular pathogen *Chlamydia trachomatis* (Al-Younes et al., 2011), indicating that lipidation of LC3 is not a strict prerequisite for its recruitment to membranes. Nevertheless, we found that SAR405 blocked the recruitment of LC3 to phagosomes, in line with the notion that the lipidation of LC3 downstream of PI(3)P-kinase VPS34 is a requirement for LAP (Martinez et al., 2015; Masud et al., 2019b) and the finding that SAR405 reduces the number of cells with LAPosomes in human macrophages (Ligeon et al., 2021). Our finding that the VPS34 inhibitor SAR405 blocks both LC3-II formation and LC3 recruitment to phagosomes is therefore consistent with the literature. Our finding that SAR405 inhibits the phagocytotic uptake is also in line with previous findings that this compound inhibits endocytosis (Filippakis et al., 2018; Ronan et al., 2014). Independent of its role in autophagy and LAP, VPS34 is well known to promote endocytosis and endosomal maturation (Backer, 2016; Yoshioka, 2021). Since many of the cellular mechanisms of phagocytotic uptake and maturation are shared with endocytic uptake and maturation (Fairn and Grinstein, 2012), it is therefore no surprise that inhibition of VPS34 inhibits phagocytosis as well. In fact, similar to LAP, endocytosis can in some cases also depend

on the direct conjugation of LC3 to early endosomal membranes, where it plays a role in the recycling of the receptors CD36 and TREM2 from endosomes to the plasma membrane (Heckmann et al., 2019).

We found that EACC treatment of monocyte-derived DCs results in decreased cellular levels of total LC3, irrespective of its lipidation state, and both in the presence and absence of zymosan. These findings contradict earlier results in HeLa cells, where EACC treatment resulted in elevated levels of LC3-II upon starvation and the levels of LC3-I were not affected (Vats and Manjithaya, 2019). This discrepancy might be well explained by the differences between cell types, as it has been shown that both expression levels of LC3 (Tanida et al., 2005) and LC3 flux (Klionsky et al., 2021) can vary widely among different cell types. For instance, serum starvation or rapamycin treatment has been reported to result both in an increase (Cai et al., 2010; Castino et al., 2011; Gui et al., 2019; Tanida et al., 2005) and a decrease (Mizushima et al., 2004) of LC3-II in different cell types. In monocyte-derived DCs, we found that starvation reduces LC3-I levels and experiments with the ribosomal inhibitor CHX showed a rapid turnover of LC3. Since EACC did not further reduce cellular levels of LC3 in starvation medium, and EACC also did not reduce LC3 levels in the presence of serum, EACC seems to accelerate LC3 turnover. This turnover is not caused by degradation of LC3 in acidic lysosomes, since treating the cells with a combination of both EACC and bafilomycin A1 also resulted in lower levels of total LC3, showing that this reduction is independent of lysosomal acidification. However, EACC did not significantly reduce LC3 levels in the presence of the proteasomal inhibitor MG132, suggesting that LC3 was degraded by the proteasome. Thus, our data suggest that EACC seems to accelerate the turnover of LC3 by proteasomal degradation. Indeed, it has previously been shown that LC3 is degraded by the proteasome following ubiquitination (Jia and Bonifacino, 2019).

A possible explanation of why EACC would exert different effects in different cell types are the multiple trafficking roles of Stx17. In addition to the fusion of autophagosomes with lysosomes, Stx17 has roles in endocytosis (Dingjan et al., 2018) and Golgi transport (Itakura et al., 2012; Jahn and Fasshauer, 2012; Muppirala et al., 2011) and is present on phagosomes (Dingjan et al., 2018). Indeed, our data suggest that EACC might also target fusion events required for $gp91^{phox}$ recruitment to phagosomes, possibly phagosome-lysosome fusion (Dingjan et al., 2017). The contribution of Stx17 to different trafficking routes might well vary among cell types and/or conditions of nutrient availability, which might well explain why its inhibition by EACC would result in different outcomes. Thus, perhaps the blockage of Stx17 by EACC disrupts the endoplasmic reticulum, Golgi and/or endosomal trafficking in human monocyte-derived DCs (but not or less in starved HeLa cells), leading to the accelerated degradation of LC3.

Our finding that bafilomycin A1 treatment inhibits LC3 recruitment to phagosomes is in line with previous reports that inhibition of the V-ATPase does not affect LC3-II formation, but inhibits LAP (Florey et al., 2015). These findings thus strengthen the conclusion that the LC3 lipidation machinery in LAP is dependent on the activity of the V-ATPase (Florey et al., 2015; Hooper et al., 2021; Jacquin et al., 2017). The mechanism in which the V-ATPase promotes LC3 lipidation at the phagosome has been attributed to osmotic imbalance and water influx (Florey et al., 2015). It has been shown that chloroquine, which promotes such osmotic imbalance as it accumulates at high levels in the lumen of endosomes, increases the recruitment of GFP-tagged LC3 to uncoated latex bead-containing phagosomes

in the mouse macrophage-like cell line J774 (Florey et al., 2015). We therefore expected that chloroquine would also promote LC3 recruitment to zymosan-containing phagosomes. However, we found that in human monocyte-derived DCs, chloroquine did not increase the recruitment of endogenous LC3 to zymosan containing phagosomes. Instead, LC3 recruitment to phagosomes was not significantly affected by chloroquine, and was even reduced in 3 out of 4 donors. Possibly, compared to zymosan particles, the osmotic effects of chloroquine could be larger in phagosomes containing latex beads, as these phagosomes will have a relatively small aqueous volume due to the large inert core of the latex particle. However, this discrepancy might also be caused by the different cell types and/or different engagement of phagocytic uptake receptors. In addition, GFP-LC3 might be recruited in a different manner than endogenous LC3. Nevertheless, our finding is in line with findings that chloroquine did not block the recruitment of LC3 to phagosomes containing zymosan in RAW264.7 cells (Sanjuan et al., 2007) and to vacuoles containing the intracellular pathogen *L. monocytogenes* in murine peritoneal macrophages (Gluschko et al., 2018). Thus, although we could not confirm the findings that osmotic destabilization of phagosomes promotes LC3 recruitment, our findings at least confirm that whereas phagosomal LC3 recruitment is inhibited by the direct blockage of the V-ATPase by bafilomycin A1, the inhibition of acidification by chloroquine does not suffice for this.

One explanation why direct inhibition of the V-ATPase by bafilomycin A1, but not the blockage of acidification by chloroquine, results in inhibition of LAP might relate to NOX2. Production of superoxide anion by NOX2 is well-known to promote LAP (Huang et al., 2009; Ligeon et al., 2021; Martinez et al., 2015; Masud et al., 2019a). However, NOX2 counteracts the activity of the V-ATPase, as dismutation of superoxide anion produced by NOX2 sequesters protons that can even result in an increase of the pH (Savina et al., 2006). As a consequence, the V-ATPase might actually increase NOX2 activity: the V-ATPase pumps protons into the phagosome which sequester superoxide anion to form H_2O_2. This continuous removal of superoxide anion might reduce the competition between the product (superoxide anion) and the substrate (molecular oxygen) for binding to NOX2, thereby potentially facilitating higher levels or prolonged production of superoxide anion. Inhibiting the V-ATPase may therefore reduce NOX2 activity. Indeed, experiments with mouse lung endothelial cells, showed that NOX2 activity depends on the activity of the V-ATPase and can be inhibited by bafilomycin A1 (Harrison et al., 2018). Given that chloroquine is a weak base with relatively low pKa (pKa1 = 8.1, pKa2 = 10.2) (Al-Bari, 2014), this compound might not or less effectively inhibit dismutation, and thus might be less efficient in inhibiting NOX2 mediated ROS production compared to the direct inhibition of the V-ATPase. In line with this, our data show that bafilomycin A1 resulted in a (non-significant) trend towards reduced phagosomal oxidation, whereas this was increased with chloroquine.

The mechanism underlying the reduced phagosomal recruitment of LC3 and the reduced levels of phagosomal oxidation in the presence of bafilomycin A1 compared to chloroquine remains an open question. Possibly, the differences between bafilomycin A1 and chloroquine might relate to their effects on membrane trafficking. First, our data suggests that chloroquine might increase ROS production by increasing the phagosomal presence of $gp91^{phox}$, possibly due to its effects on inter-organellar trafficking (Chen et al., 2011; Mauthe et al., 2018; Wolfram et al., 2017). Second, it was recently proposed that ATP6V1A, the catalytic subunit of the V1 complex of V-ATPase, co-precipitates with ATG16L1 during LAP in RAW264.7 cells (Hooper et al., 2021), providing a direct link between the

V-ATPase and LAP, as ATG16L1 is required for LC3-lipidation (Hooper et al., 2021). The same authors show that inhibition of NADPH oxidase by diphenyleneiodonium reduces phagosomal recruitment of ATP6V1A, suggesting that NOX2 activity induces LAP by triggering increased V-ATPase recruitment (Hooper et al., 2021). It is speculated that this NOX2-induced V-ATPase recruitment is due to ROS-mediated H^+ sequestration, leading to a compensatory mechanism in which more V-ATPase is recruited to the phagosome in order to achieve acidification in spite of the H^+ sequestration (Hooper et al., 2021). As bafilomycin A1 also inhibits phagosomal acidification, this compensatory mechanism might also occur following bafilomycin A1 treatment. Third, bafilomycin A1 decreases autophagosome-lysosome fusion in rat kidney cells, as shown by a bafilomycin-induced loss of lgp120 (a marker for lysosomes and late endosomes) in LC3-positive vesicles (Jahreiss et al., 2008). In addition, bafilomycin A1 has been shown to inhibit autophagosome-lysosome fusion in *Drosophila* as shown by a decreased colocalisation of Atg8 and LAMP1 (a lysosomal marker) (Mauvezin and Neufeld, 2015; Mauvezin et al., 2015). As the sarco/endoplasmic reticulum Ca^{2+}-ATPase (SERCA) pump has been identified as a target of bafilomycin A1, and depletion of the single *Drosophila* SERCA homologue (dSERCA/CaP60A) reduced autophagosome-lysosome fusion, it has been proposed that the bafilomycin-induced fusion defect is due to the inhibition of the SERCA pump, leading to decreased Ca^{2+} transport from the cytoplasm to the ER (Mauvezin and Neufeld, 2015; Mauvezin et al., 2015). Although it is not clear yet whether the bafilomycin-induced fusion defect is caused by an elevated cytosolic Ca^{2+} concentration, a decreased Ca^{2+} concentration in the ER lumen, or both (Mauvezin and Neufeld, 2015; Mauvezin et al., 2015), these findings suggest that fusion events involving lysosomes are sensitive to bafilomycin A1-induced shifts in Ca^{2+} concentration. Thus, bafilomycin A1 might possibly decrease LAPosome-lysosome fusion as well, thereby potentially interfering with $gp91^{phox}$ recruitment and subsequent LC3 recruitment.

Not only in LAP, but also in other mechanisms involving the LC3 recruitment to single membranes the activity of the V-ATPase is linked to LC3 lipidation. For example, recently it has been shown that detection of microbial DNA by the cGAS-STING pathway induces LC3 lipidation onto single-membrane perinuclear vesicles (Gui et al., 2019). Although this process does not depend on ULK1/2 nor VPS34 (Gui et al., 2019), it could be blocked by bafilomycin A1, indicating that activation of the cGAS-STING pathway induces V-ATPase-dependent LC3 lipidation independent on VPS34 (Fischer et al., 2020).

Given the importance of LAP and autophagy in both the innate and adaptive immune responses against pathogens, there is much interest in targeting these processes by small molecule inhibitors (Pasquier, 2016), for instance for the treatment of cancer, infectious disease and autoimmune diseases (Galluzzi et al., 2017). As DCs play a central role in the initiation of the adaptive immune response against pathogens and tumour cells by antigen presentation (Bevan, 1976), and as LAP is important for antigen presentation (Ligeon et al., 2021), studying LAP in this cell type is particularly relevant. Here we show that, next to inhibiting macroautophagy, bafilomycin A1 and SAR405 inhibit LAP in human monocyte-derived DCs. In addition, we show that chloroquine does not increase LAP in human DCs, in contrast to the reported increase in the recruitment of LC3 to uncoated latex bead-containing phagosomes in the J774 macrophage cell line (Florey et al., 2015), We also shown that while EACC induces a decrease in LC3-II in starved HeLa cells (Vats and Manjithaya, 2019), this is not the case in starved DCs. Thereby, our data highlights the

importance of testing inhibitors for their effects on autophagy and LAP in different cell types, in a field where most studies have focussed on macrophages so far. To expand the knowledge on how to target LAP and autophagy in specific diseases, the functional effects of different types of stimuli or phagocytic cargoes combined with different inhibitors of autophagy and LAP should be studied in the future.

Data availability

The data that support the findings of this study are openly available in Zenodo at https://zenodo.org/deposit/5714530#, DOI: 10.5281/zenodo.5714530.

Acknowledgements

G.v.d.B. is funded by a Young Investigator Grant from the Human Frontier Science Program (HFSP; RGY0080/2018). G.v.d.B has received funding from the European Research Council (ERC) under the European Union's Horizon 2020 research and innovation programme (grant agreement No. 862137).

References

Al-Bari, A.A. (2014). Chloroquine analogues in drug discovery: New directions of uses, mechanisms of actions and toxic manifestations from malaria to multifarious diseases. J. Antimicrob. Chemother. *70*, 1608–1621.

Al-Younes, H.M., Al-Zeer, M.A., Khalil, H., Gussmann, J., Karlas, A., Machuy, N., Brinkmann, V., Braun, P.R., and Meyer, T.F. (2011). Autophagy-independent function of MAP-LC3 during intracellular propagation of Chlamydia trachomatis. Autophagy *7*, 814–828.

Alvarez, Y., Municio, C., Alonso, S., San Román, J.A., Sánchez Crespo, M., and Fernández, N. (2009). Cyclooxygenase-2 Induced by Zymosan in Human Monocyte-Derived Dendritic Cells Shows High Stability, and Its Expression Is Enhanced by Atorvastatin. J. Pharmacol. Exp. Ther. *329*, 987–994.

Backer, J.M. (2016). The intricate regulation and complex functions of the Class III phosphoinositide 3-kinase Vps34. Biochem. J. *473*, 2251–2271.

Baranov, M. V., Bianchi, F., Schirmacher, A., van Aart, M.A.C., Maassen, S., Muntjewerff, E.M., Dingjan, I., ter Beest, M., Verdoes, M., Keyser, S.G.L., et al. (2019). The Phosphoinositide Kinase PIKfyve Promotes Cathepsin-S-Mediated Major Histocompatibility Complex Class II Antigen Presentation. IScience *11*, 160–177.

Bevan, M.J. (1976). Minor H Antigens Introduced on H-2 Different Stimulating Cells Cross-React at the Cytotoxic T Cell Level during in Vivo Priming. J. Immunol. *117*.

Bowman, E.J., Siebers, A., and Altendorf, K. (1988). Bafilomycins; A class of inhibitors of membrane ATPases from microorganisms, animal cells, and plant cells. Proc. Natl. Acad. Sci. U. S. A. *85*, 7972–7976.

Cai, Q., Lu, L., Tian, J.H., Zhu, Y.B., Qiao, H., and Sheng, Z.H. (2010). Snapin-regulated late endosomal transport is critical for efficient autophagy-lysosomal function in neurons. Neuron *68*, 73–86.

Castino, R., Fiorentino, I., Cagnin, M., Giovia, A., and Isidoro, C. (2011). Chelation of lysosomal iron protects dopaminergic SH-SY5Y neuroblastoma cells from hydrogen peroxide toxicity by precluding autophagy and Akt dephosphorylation. Toxicol. Sci. *123*, 523–541.

Chen, P.M., Gombart, Z.J., and Chen, J.W. (2011). Chloroquine treatment of ARPE-19 cells leads to lysosome dilation and intracellular lipid accumulation: Possible implications of lysosomal dysfunction in macular degeneration. Cell Biosci. *1*, 1–10.

Cunha, L.D., Yang, M., Carter, R., Guy, C., Harris, L., Crawford, J.C., Quarato, G., Boada-Romero, E., Kalkavan, H., Johnson, M.D.L., et al. (2018). LC3-Associated Phagocytosis in Myeloid Cells Promotes Tumor Immune Tolerance. Cell *175*, 429-441.e16.

Dingjan, I., Linders, P.T.A., Bekerom, L. van den, Baranov, M. V., Halder, P., ter Beest, M., and van den Bogaart, G. (2017). Oxidized phagosomal NOX2 complex is replenished from lysosomes. J. Cell Sci. *130*, 1285–1298.

Dingjan, I., Linders, P.T.A., Verboogen, D.R.J., Revelo, N.H., Ter Beest, M., and Van Den Bogaart, G. (2018). Endosomal and phagosomal SNAREs. Physiol. Rev. *98*, 1465–1492.

Durgan, J., Lystad, A.H., Sloan, K., Carlsson, S.R., Wilson, M.I., Marcassa, E., Ulferts, R., Webster, J., Lopez-Clavijo, A.F., Wakelam, M.J., et al. (2021). Non-canonical autophagy drives alternative ATG8 conjugation to phosphatidylserine. Mol. Cell *81*, 2031-2040.e8.

Fairn, G.D., and Grinstein, S. (2012). How nascent phagosomes mature to become phagolysosomes. Trends Immunol. *33*, 397–405.

Fazeli, G., and Wehman, A.M. (2017). Safely removing cell debris with LC3-associated phagocytosis. Biol. Cell *109*, 355–363.

Filippakis, H., Belaid, A., Siroky, B., Wu, C., Alesi, N., Hougard, T., Nijmeh, J., Lam, H.C., and Henske, E.P. (2018). Vps34-mediated macropinocytosis in Tuberous Sclerosis Complex 2-deficient cells supports tumorigenesis. Sci. Rep. *8*.

Fischer, T.D., Wang, C., Padman, B.S., Lazarou, M., and Youle, R.J. (2020). STING induces LC3B lipidation onto single-membrane vesicles via the V-ATPase and ATG16L1-WD40 domain. J. Cell Biol. *219*.

Florey, O., Gammoh, N., Kim, S.E., Jiang, X., and Overholtzer, M. (2015). V-ATPase and osmotic imbalances activate endolysosomal LC3 lipidation. Autophagy *11*, 88–99.

Galluzzi, L., Bravo-San Pedro, J.M., Levine, B., Green, D.R., and Kroemer, G. (2017). Pharmacological modulation of autophagy: Therapeutic potential and persisting obstacles. Nat. Rev. Drug Discov. *16*, 487–511.

Gluschko, A., Herb, M., Wiegmann, K., Krut, O., Neiss, W.F., Utermöhlen, O., Krönke, M., and Schramm, M. (2018). The β2 Integrin Mac-1 Induces Protective LC3-Associated Phagocytosis of Listeria monocytogenes. Cell Host Microbe *23*, 324-337.e5.

Gui, X., Yang, H., Li, T., Tan, X., Shi, P., Li, M., Du, F., and Chen, Z.J. (2019). Autophagy induction via STING trafficking is a primordial function of the cGAS pathway. Nature *567*, 262–266.

Guo, B., Liang, Q., Li, L., Hu, Z., Wu, F., Zhang, P., Ma, Y., Zhao, B., Kovács, A.L., Zhang, Z., et al. (2014). O-GlcNAc-modification of SNAP-29 regulates autophagosome maturation. Nat. Cell Biol. *16*, 1215–1226.

Harrison, I.P., Vinh, A., Johnson, I.R.D., Luong, R., Drummond, G.R., Sobey, C.G., Tiganis, T., Williams, E.D., O'Leary, J.J., Brooks, D.A., et al. (2018). NOX2 oxidase expressed in endosomes promotes cell proliferation and prostate tumour development. Oncotarget *9*, 35378–35393.

Hayashi, K., Taura, M., and Iwasaki, A. (2018). The interaction between IKKα and LC3 promotes type i interferon production through the TLR9-containing LAPosome. Sci. Signal. *11*.

Heckmann, B.L., Teubner, B.J.W., Tummers, B., Guy, C.S., Zakharenko, S.S., and Green Correspondence, D.R. (2019). LC3-Associated Endocytosis Facilitates β-Amyloid Clearance and Mitigates Neurodegeneration in Murine Alzheimer's Disease. Cell *178*, 536-551.e14.

Herb, M., Gluschko, A., and Schramm, M. (2020). LC3-associated phagocytosis - The highway to hell for phagocytosed microbes. Semin. Cell Dev. Biol. *101*, 68–76.

Hooper, K.M., Jacquin, E., Li, T., Goodwin, J.M., Brumell, J.H., Durgan, J., and Florey, O. (2021). V-ATPase is a universal regulator of LC3 associated phagocytosis and non-canonical autophagy. BioRxiv 2021.05.20.444917.

Huang, J., Canadien, V., Lam, G.Y., Steinberg, B.E., Dinauer, M.C., Magalhaes, M.A.O., Glogauer, M., Grinstein, S., and Brumell, J.H. (2009). Activation of antibacterial autophagy by NADPH oxidases. Proc. Natl. Acad. Sci. U. S. A. *106*, 6226–6231.

Itakura, E., Kishi-Itakura, C., and Mizushima, N. (2012). The hairpin-type tail-anchored SNARE syntaxin 17 targets to autophagosomes for fusion with endosomes/lysosomes. Cell *151*, 1256–1269.

Jacquin, E., Leclerc-Mercier, S., Judon, C., Blanchard, E., Fraitag, S., and Florey, O. (2017). Pharmacological modulators of autophagy activate a parallel noncanonical pathway driving unconventional LC3 lipidation. Autophagy *13*, 854–867.

Jahn, R., and Fasshauer, D. (2012). Molecular machines governing exocytosis of synaptic vesicles. Nature *490*, 201–207.

Jahreiss, L., Menzies, F.M., and Rubinsztein, D.C. (2008). The itinerary of autophagosomes: From peripheral formation to kiss-and-run fusion with lysosomes. Traffic *9*, 574–587.

Jia, R., and Bonifacino, J.S. (2019). Negative regulation of autophagy by uba6-birc6–mediated ubiquitination of lc3. Elife *8*.

Klionsky, D.J., Abdel-Aziz, A.K., Abdelfatah, S., Abdellatif, M., Abdoli, A., Abel, S., Abeliovich, H., Abildgaard, M.H., Abudu, Y.P., Acevedo-Arozena, A., et al. (2021). Guidelines for the use and interpretation of assays for monitoring autophagy (4th edition). Autophagy *17*.

Lamprinaki, D., Beasy, G., Zhekova, A., Wittmann, A., James, S., Dicks, J., Iwakura, Y., Saijo, S., Wang, X., Chow, C.-W., et al. (2017). LC3-Associated Phagocytosis Is Required for Dendritic Cell Inflammatory Cytokine Response to Gut Commensal Yeast Saccharomyces cerevisiae. Front. Immunol. *0*, 1397.

Ligeon, L.A., Pena-Francesch, M., Vanoaica, L.D., Núñez, N.G., Talwar, D., Dick, T.P., and Münz, C. (2021). Oxidation inhibits autophagy protein deconjugation from phagosomes to sustain MHC class II restricted antigen presentation. Nat. Commun. *12*, 1–13.

Livak, K.J., and Schmittgen, T.D. (2001). Analysis of Relative Gene Expression Data Using Real-Time Quantitative PCR and the 2−ΔΔCT Method. Methods *25*, 402–408.

Martinez, J., Almendinger, J., Oberst, A., Ness, R., Dillon, C.P., Fitzgerald, P., Hengartner, M.O., and Green, D.R. (2011). Microtubule-associated protein 1 light chain 3 alpha (LC3)-associated phagocytosis is required for the efficient clearance of dead cells. Proc. Natl. Acad. Sci. U. S. A. *108*, 17396–17401.

Martinez, J., Malireddi, R.K.S., Lu, Q., Cunha, L.D., Pelletier, S., Gingras, S., Orchard, R., Guan, J.L., Tan, H., Peng, J., et al. (2015). Molecular characterization of LC3-associated phagocytosis reveals distinct roles for Rubicon, NOX2 and autophagy proteins. Nat. Cell Biol. *17*, 893–906.

Martinez, J., Cunha, L.D., Park, S., Yang, M., Lu, Q., Orchard, R., Li, Q.Z., Yan, M., Janke, L., Guy, C., et al. (2016). Noncanonical autophagy inhibits the autoinflammatory, lupus-like response to dying cells. Nature *533*, 115–119.

Masud, S., Prajsnar, T.K., Torraca, V., Lamers, G.E.M., Benning, M., Van Der Vaart, M., and Meijer, A.H. (2019a). Macrophages target Salmonella by Lc3-associated phagocytosis in a systemic infection model. Autophagy *15*, 796–812.

Masud, S., van der Burg, L., Storm, L., Prajsnar, T.K., and Meijer, A.H. (2019b). Rubicon-Dependent Lc3 Recruitment to Salmonella-Containing Phagosomes Is a Host Defense Mechanism Triggered Independently From Major Bacterial Virulence Factors. Front. Cell. Infect. Microbiol. *9*, 279.

Mauthe, M., Orhon, I., Rocchi, C., Zhou, X., Luhr, M., Hijlkema, K.J., Coppes, R.P., Engedal, N., Mari, M., and Reggiori, F. (2018). Chloroquine inhibits autophagic flux by decreasing autophagosome-lysosome fusion. Autophagy *14*, 1435–1455.

Mauvezin, C., and Neufeld, T.P. (2015). Bafilomycin A1 disrupts autophagic flux by inhibiting both V-ATPase-dependent acidification and Ca-P60A/SERCA-dependent autophagosome-lysosome fusion. Autophagy *11*, 1437–1438.

Mauvezin, C., Nagy, P., Juhász, G., and Neufeld, T.P. (2015). Autophagosome-lysosome fusion is independent of V-ATPase-mediated acidification. Nat. Commun. *6*.

Mizushima, N., Yamamoto, A., Matsui, M., Yoshimori, T., and Ohsumi, Y. (2004). In Vivo Analysis of Autophagy in Response to Nutrient Starvation Using Transgenic Mice Expressing a Fluorescent Autophagosome Marker. Mol. Biol. Cell *15*, 1101–1111.

Muppirala, M., Gupta, V., and Swarup, G. (2011). Syntaxin 17 cycles between the ER and ERGIC and is required to maintain the architecture of ERGIC and Golgi. Biol. Cell *103*, 333–350.

Pasquier, B. (2016). Autophagy inhibitors. Cell. Mol. Life Sci. *73*, 985–1001.

Poole, B., and Ohkuma, S. (1981). Effect of Weak Bases on the Intralysosomal pH in Mouse Peritoneal Macrophages Lysosomal pH Measurement.

Romao, S., Gasser, N., Becker, A.C., Guhl, B., Bajagic, M., Vanoaica, D., Ziegler, U., Roesler, J., Dengjel, J., Reichenbach, J., et al. (2013). Autophagy proteins stabilize pathogen-containing phagosomes for prolonged MHC II antigen processing. J. Cell Biol. *203*, 757–766.

Ronan, B., Flamand, O., Vescovi, L., Dureuil, C., Durand, L., Fassy, F., Bachelot, M.F., Lamberton, A., Mathieu, M., Bertrand, T., et al. (2014). A highly potent and selective Vps34 inhibitor alters vesicle trafficking and autophagy. Nat. Chem. Biol. *10*, 1013–1019.

Sanjuan, M.A., Dillon, C.P., Tait, S.W.G., Moshiach, S., Dorsey, F., Connell, S., Komatsu, M., Tanaka, K., Cleveland, J.L., Withoff, S., et al. (2007). Toll-like receptor signalling in macrophages links the autophagy pathway to phagocytosis. Nature *450*, 1253–1257.

Savina, A., Jancic, C., Hugues, S., Guermonprez, P., Vargas, P., Moura, I.C., Lennon-Duménil, A.M., Seabra, M.C., Raposo, G., and Amigorena, S. (2006). NOX2 Controls Phagosomal pH to Regulate Antigen Processing during Crosspresentation by Dendritic Cells. Cell *126*, 205–218.

Tanida, I., Minematsu-Ikeguchi, N., Ueno, T., and Kominami, E. (2005). Lysosomal turnover, but not a cellular level, of endogenous LC3 is a marker for autophagy. Autophagy *1*, 84–91.

Vats, S., and Manjithaya, R. (2019). A reversible autophagy inhibitor blocks autophagosome–lysosome fusion by preventing Stx17 loading onto autophagosomes. Mol. Biol. Cell *30*, 2283–2295.

Verboogen, D.R.J., Revelo, N.H., Ter Beest, M., and Van Den Bogaart, G. (2019). Interleukin-6 secretion is limited by self-signaling in endosomes. J. Mol. Cell Biol. *11*, 144.

Wolfram, J., Nizzero, S., Liu, H., Li, F., Zhang, G., Li, Z., Shen, H., Blanco, E., and Ferrari, M. (2017). A chloroquine-induced macrophage-preconditioning strategy for improved nanodelivery. Sci. Rep. *7*, 1–13.

Wong, S.W., Sil, P., and Martinez, J. (2018). Rubicon: LC3-associated phagocytosis and beyond. FEBS J. *285*, 1379–1388.

Wu, M.Y., and Lu, J.H. (2019). Autophagy and Macrophage Functions: Inflammatory Response and Phagocytosis. Cells *9*.

Xu, J., Feng, H.T., Wang, C., Yip, K.H.M., Pavlos, N., Papadimitriou, J.M., Wood, D., and Zheng, M.H. (2003). Effects of bafilomycin A1: An inhibitor of vacuolar H (+)-ATPases on endocytosis and apoptosis in RAW cells and RAW cell-derived osteoclasts. J. Cell. Biochem. *88*, 1256–1264.

Yang, C.S., Lee, J.S., Rodgers, M., Min, C.K., Lee, J.Y., Kim, H.J., Lee, K.H., Kim, C.J., Oh, B., Zandi, E., et al. (2012). Autophagy protein rubicon mediates phagocytic NADPH oxidase activation in response to microbial infection or TLR stimulation. Cell Host Microbe *11*, 264–276.

Yoshioka, K. (2021). Class II phosphatidylinositol 3-kinase isoforms in vesicular trafficking. Biochem. Soc. Trans. *49*, 893–901.

Figure legends

Figure 1. Autophagy inhibitors differently affect LC3 lipidation and total cellular LC3 levels. (A) Monocyte-derived dendritic cells (moDCs) were incubated for 4 hours with 250 nM bafilomycin A1 (baf A1) and increasing concentrations of SAR405 followed by stimulation with zymosan particles. Control conditions were also included as indicated. One-way ANOVA followed by post hoc Tukey for the four samples on the left and two-way ANOVA followed by post-hoc Dunnett's for the SAR405 concentration series. **(B)** Representative western blot analysis of moDCs incubated with either 250 nM bafilomycin A1 (baf A1) or 25 μM chloroquine (CQ) at the indicated time points. **(C)** Comparison of the effects of 250 nM bafilomycin A1 (baf A1) and increasing concentrations of EACC on LC3 levels. One-way ANOVA followed by post-hoc Tukey for the four samples on the left and two-way ANOVA followed by post-hoc Dunnett's for the EACC concentration series. **(D)** Combined effect of baf A1 and increasing concentrations of EACC on LC3 cellular levels. Graph shows average levels ± SD of LC3-I (gray) and LC3-II (black) corrected for loading control (GAPDH or tubulin) and normalized to the condition with bafilomycin A1 and zymosan. Blots of the other donors are in Supplementary Fig. 2. ∗: $P < 0.05$; ∗∗: $P < 0.01$; ∗∗∗: $P < 0.001$; ∗∗∗∗: $P < 0.0001$; ns: not significant.

Figure 2. LC3 is recruited to the single membrane of the phagosome. **(A)** Confocal image of monocyte-derived dendritic cell incubated with zymosan particles for two hours showing a phagosome with immunostaining for LC3

(yellow), actin (magenta) and DAPI and Alexa Fluor 405-labeled zymosan (cyan). Zoom of phagosome is shown in inset. BF: bright field. Scale bar: 10 µm. **(B)** High-pressure cryo-fixation electron microscopy micrograph of moDC incubated with zymosan particles for two hours. Four zymosan particles are shown, indicated with asterisks. Samples were immunogold labeled for LC3. The bottom panel shows a close-up of the area marked with the white rectangle in the top panel. Gold particles localized at the single membrane of the phagosome are indicated with arrows. Scale bars: 1 µm.

Figure 3. Bafilomycin A1, SAR405 and chloroquine inhibit phagocytosis whereas EACC does not. (A) Flow cytometry gating strategy to identify percentage of monocyte-derived dendritic cells (moDCs) phagocytosing zymosan particles. MoDCs were selected by gating on forward scatter (FSC) and side scatter (SSC). Doublets were omitted by gating out events with a low FSC-height (H)/FSC-area (A) ratio. Living cells were selected by gating on events with a low intensity for the viability dye eFluor780. Then, cells were gated for zymosan-AF405 (Zym) signal. **(B)** The percentage and mean fluorescence intensity (MFI) of zymosan-positive cells in the presence of 100 nM bafilomycin A1 (baf A1), 10 µM SAR405 (SAR), 25 µM chloroquine (CQ) or 5 µM EACC were plotted for 3 to 7 different donors per condition. Student's paired two-sided t-tests. ∗∗: $P < 0.01$; ∗∗∗: $P < 0.001$; ns: not significant.

Figure 4. LC3 and gp91^{phox} recruitment to phagosomes. (A) Confocal images showing monocyte-derived dendritic cells stimulated with zymosan and immunolabeled for gp91^{phox} (magenta in merge) and LC3 (yellow in merge). Images show representative phagosomes that are either positive for both gp91^{phox} and LC3, only positive for LC3, only positive for gp91^{phox}, or double negative. The inset in each condition shows a representative phagosome. BF: bright field. DAPI and zymosan in cyan. Scale bar: 10 µm. **(B)** Quantification of phagosome distribution according to the conditions shown in panel (A). Cells were stimulated with zymosan A for 15, 30, 45, 60 or 120 minutes. Percentages are normalized to the total amount of phagosomes. The graph represents mean ± S.D. for the different time points from 4 different donors. **(C)** Scatter plot showing relative LC3-intensity and gp91^{phox}-intensity from the phagosomes quantified in panel (B) for the 4 different donors. Phagosomes of all time points were pooled. Lines represent the linear regression analysis for each donor.

Figure 5. Bafilomycin A1 and SAR405 inhibit LC3-recruitment to the phagosome. (A) Representative confocal images of zymosan-pulsed monocyte-derived dendritic cells (moDCs) treated with 100 nM bafilomycin A1 (baf A1), 10 µM SAR405, 25 µM chloroquine (CQ) or 5 µM EACC. Immunofluorescence staining for gp91^{phox} (magenta in merge) and LC3 (yellow in merge). DMSO: vehicle control. BF: bright field. DAPI and zymosan in cyan. Scale bar, 10 µm. **(B)** Quantification of gp91^{phox} signal at phagosomal membrane and percentage of gp91^{phox}-positive phagosomes from panel (A). Analysis in Supplementary Fig. 6. **(C)** Same as panel (B), but now for LC3. Student's paired two-sided t-tests. ∗: $P < 0.05$; ∗∗: $P < 0.01$; ns: not significant.

Figure 6. EACC reduces phagosomal oxidation, whereas chloroquine increases phagosomal oxidation relative to bafilomycin A1. (A) Flow cytometry gating strategy to select monocyte-derived dendritic cells (moDCs) phagocytosing zymosan particles labeled with the oxidation probe Bodipy581/591 C11. MoDCs were selected by

gating the forward scatter (FSC) and side scatter (SSC) signals. Doublets were omitted by gating out events with a low FSC-height (H)/FSC-area (A) ratio. Living cells were selected by gating on events with a low intensity for the viability dye eFluor780. Then, the fluorescence signal of the oxidized probe was measured in the FITC channel, and of the non-oxidize probe in the PE-channel. Shown are representative histograms for moDCs treated with 100 µM of the antioxidant α-tocopherol (α-toco) and DMSO (solvent control) as positive and negative controls, respectively. **(B)** The ratios of signals in the FITC over PE channels from panel (A) as a measure for phagosomal oxidation. Cells from 7 donors were treated with DMSO (solvent control), 100 µM α-toco, 100 nM bafilomycin A1 (baf A1), 10 µM SAR405 (SAR), 25 µM chloroquine (CQ) or 5 µM EACC. Paired sample T-tests. ∗: $P < 0.05$; ∗∗∗: $P < 0.001$; ns: not significant.

Figure 7. Inhibitors of the canonical autophagy and LC3-associated phagocytosis pathways and their targets. **(A)** Canonical autophagy is initiated by activation of the ULK1/2 complex and its recruitment to the site of phagophore initiation, where it phosphorylates the phosphatidylinositol 3-kinase catalytic subunit type 3 (PI3KC3) complex. The catalytic subunit of this complex, VPS34, phosphorylates phosphatidylinositol (PI) thereby generating phosphatidylinositol 3-phosphate (PI(3)P) which is required for the recruitment of autophagy proteins responsible for LC3-lipidation at the phagophore. After completion of the double membrane autophagosome, the V-ATPase is delivered by fusion of lysosomes with the outer membrane. Acidification results in degradation of the lumen with the inner membrane including LC3. LC3 at the outer membrane is delipidated by ATG4 and is recycled. **(B)** LC3-associated phagocytosis (LAP) is initiated by receptor-mediated uptake of particles (e.g., zymosan) but, in contrast to canonical autophagy, the resulting LAPosomes consist of a single membrane. Although LAP also requires of the PI3KC3 complex for (PI(3)P) formation, the complex composition is slightly different. For example, it contains Rubicon which is required to stabilize the NOX2 complex and for the activity of the PI3KC3 complex (Martinez et al., 2015). As there is no inner membrane containing LC3, LAP does not entail degradation of LC3. SAR405 inhibits VPS34 (Ronan et al., 2014), bafilomycin inhibits the V-ATPase (Bowman et al., 1988), chloroquine is a lysosomotropic base (Al-Bari, 2014) and EACC inhibits the loading of syntaxin 17 (Stx17) onto autophagosomes (Vats and Manjithaya, 2019). TLR: toll-like receptor. Created with BioRender.com.

Figure 1

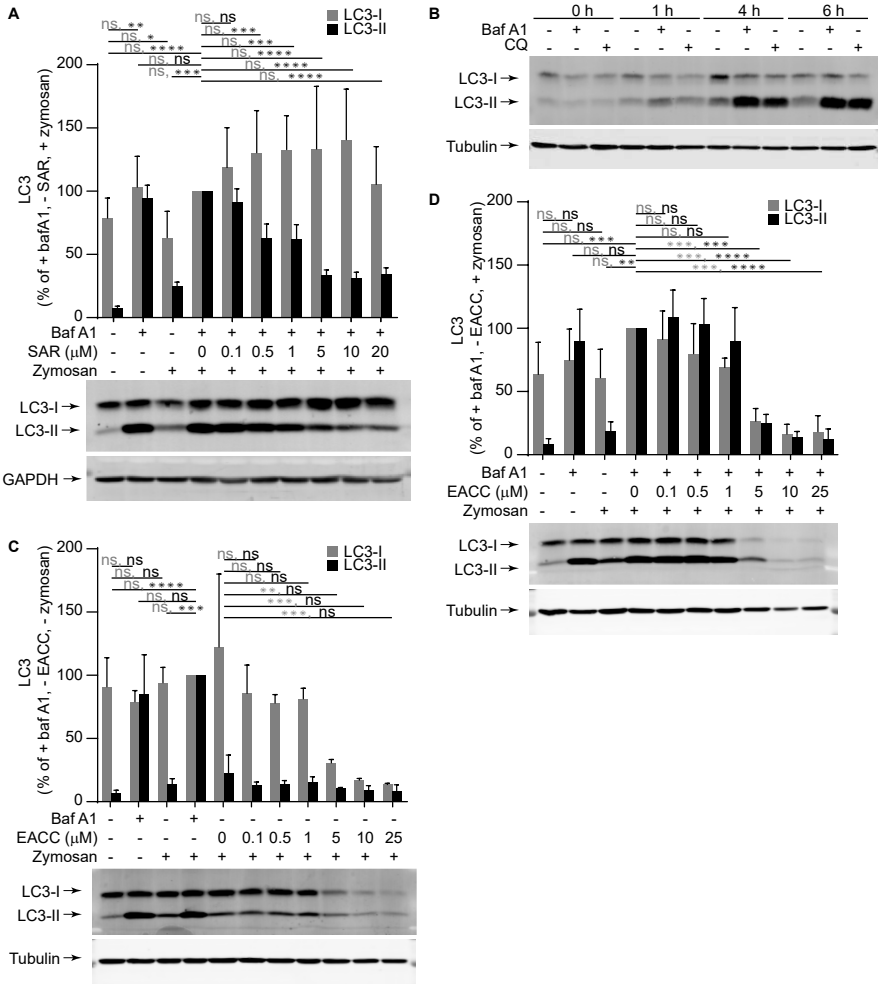

Figure 2

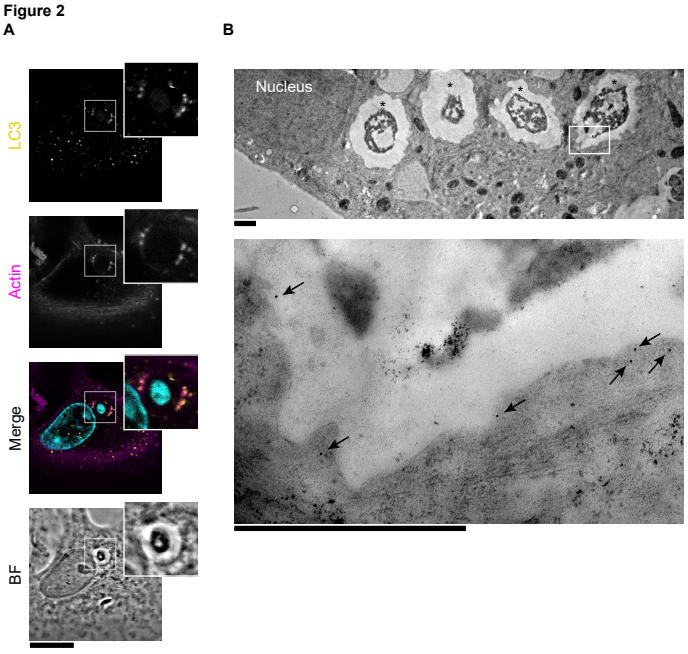

Figure 3

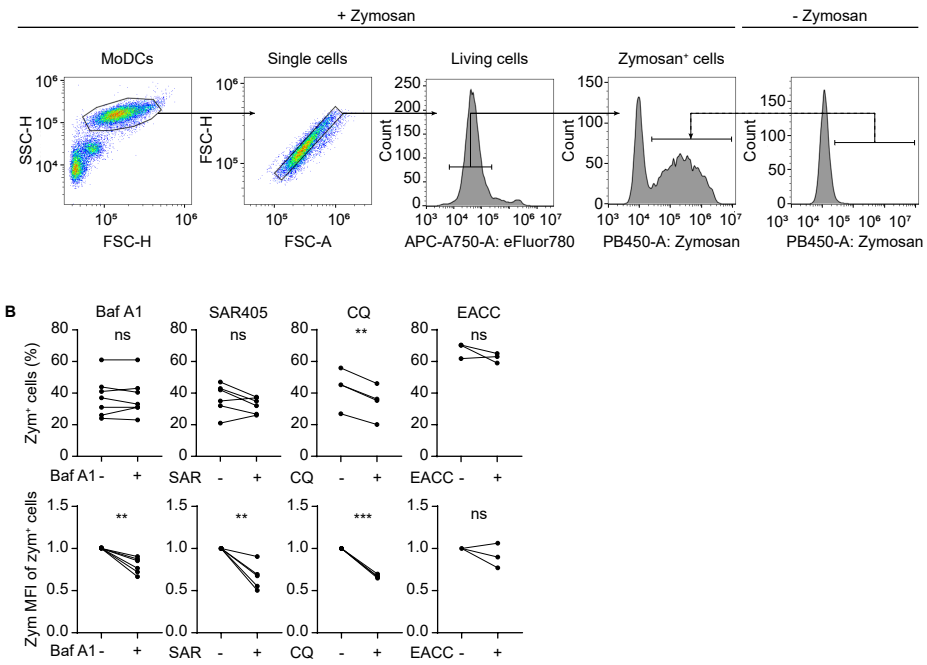

Figure 4

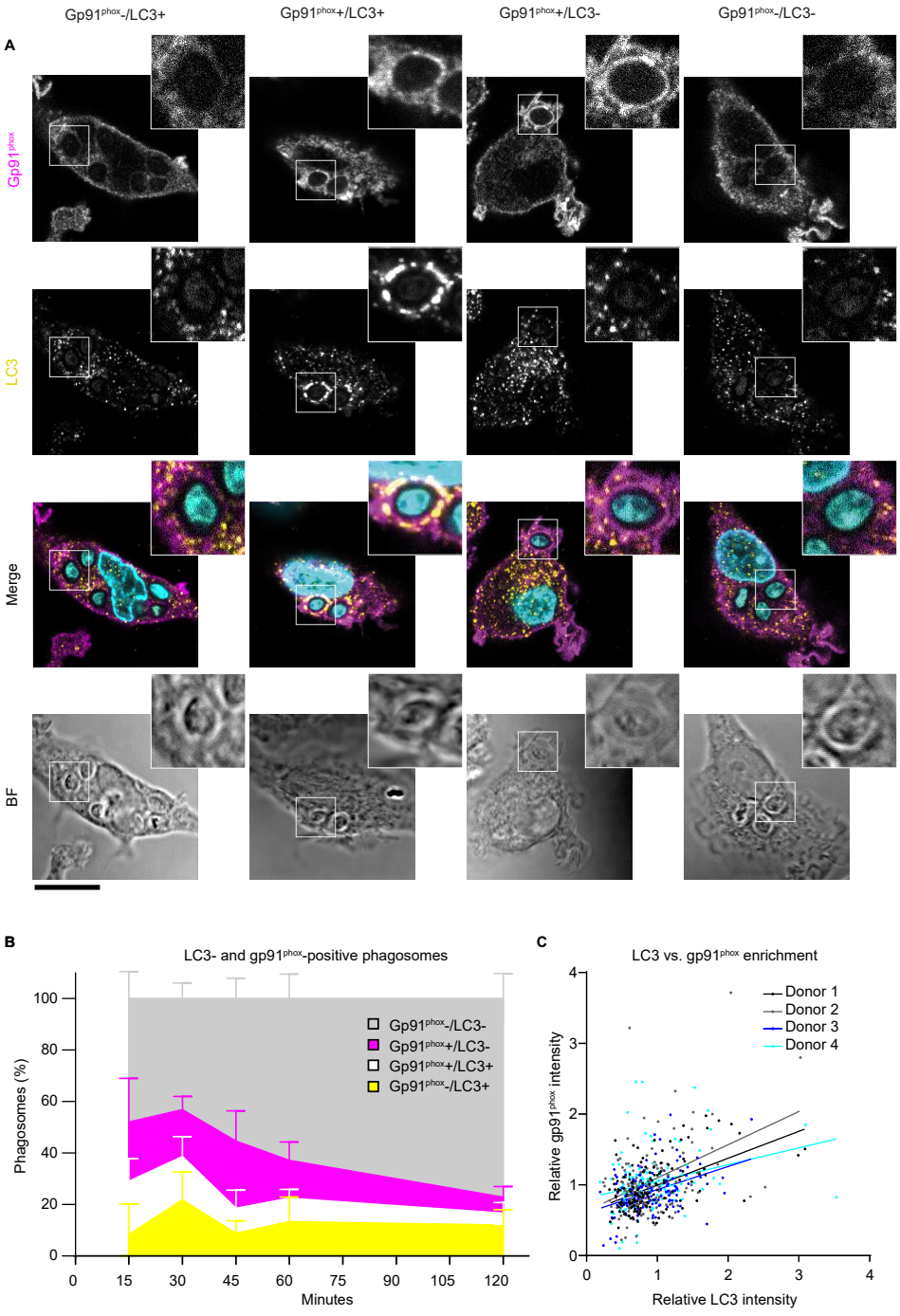

Figure 5

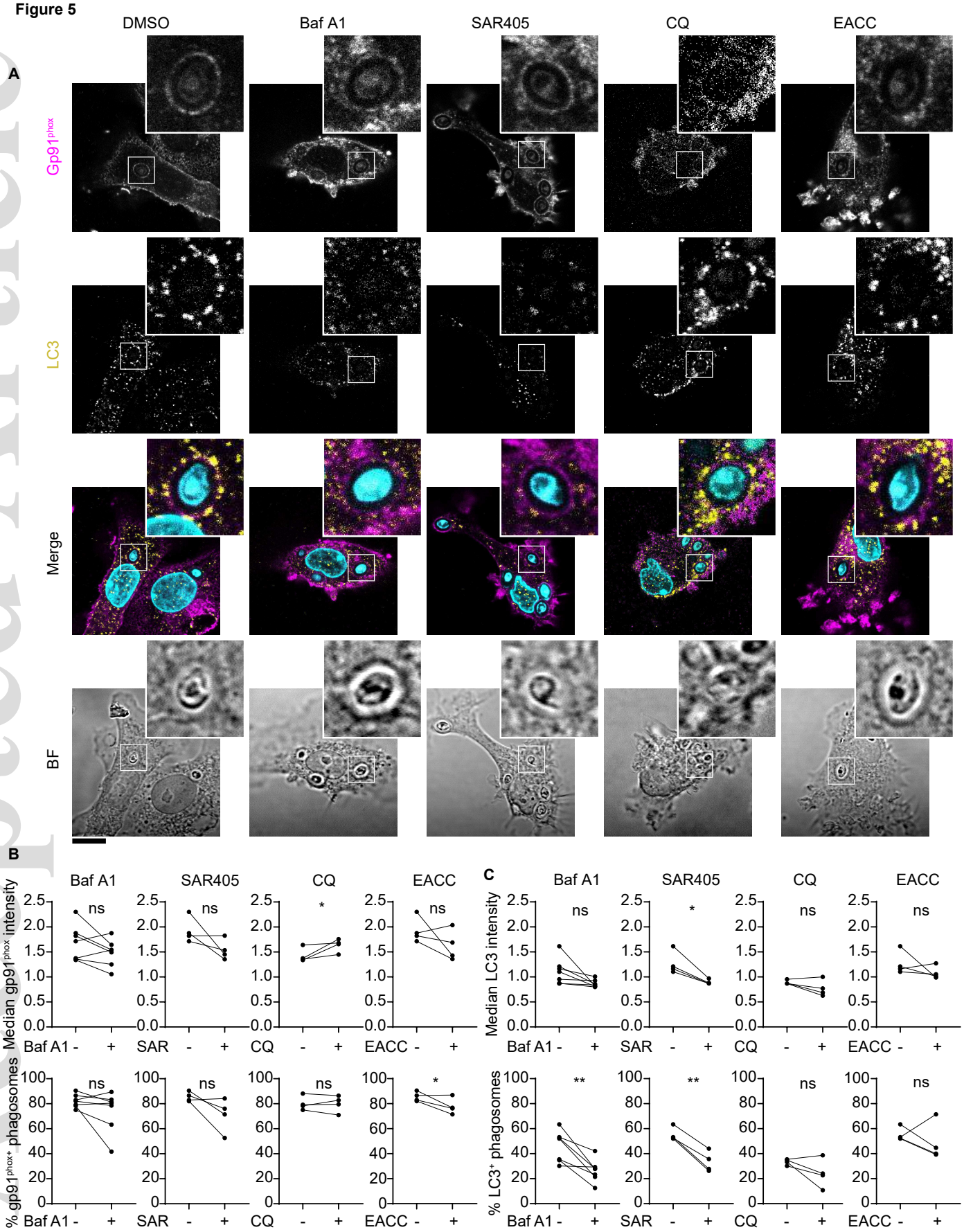

Figure 6

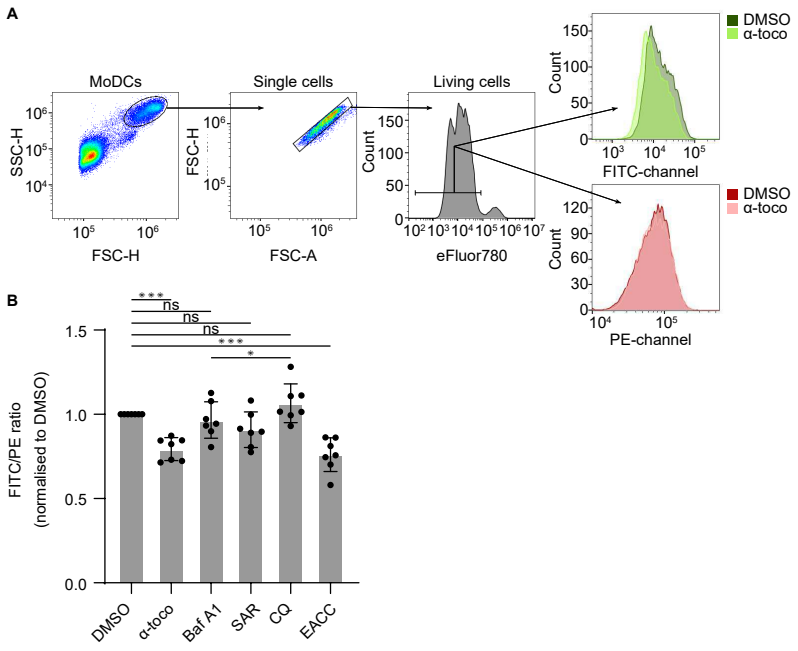

Figure 7